Long-term evolution of spherical shell with boron carbide layer after explosive compression

A. V. Andriyash, V. A. Arinin, S. A. Dyachkov (iD), G. Ya Karpenko, V. V. Kovaldov, P. Yu Korotaev (iD), S. E. Kuratov, S. A. Medin (iD), A. L. Mikhailov, S. A. Murzov (iD), A. V. Nefedov, K. N. Panov, A. N. Parshikov, S. Yu Sogrin, A. V. Yanilkin, and V. V. Zhakhovsky (iD)

View Online   Export Citation   CrossMark

Long-term evolution of spherical shell with boron carbide layer after explosive compression

View Online · Export Citation · CrossMark

A. V. Andriyash,[1] V. A. Arinin,[2] S. A. Dyachkov,[1,3,4,a]) (ID) G. Ya Karpenko,[2] V. V. Kovaldov,[2] P. Yu Korotaev,[1] (ID)
S. E. Kuratov,[1] S. A. Medin,[3,4] (ID) A. L. Mikhailov,[2] S. A. Murzov,[1,3] (ID) A. V. Nefedov,[2] K. N. Panov,[2] A. N. Parshikov,[1,4]
S. Yu Sogrin,[2] A. V. Yanilkin,[1,3] and V. V. Zhakhovsky[1] (ID)

AFFILIATIONS

[1]Dukhov Research Institute of Automatics, 22 Sushchevskaya St., Moscow 127055, Russia
[2]Russian Federal Nuclear Center, All-Russia Research Institute of Experimental Physics, Sarov, Nizhegorodskaya oblast' 607188, Russia
[3]Moscow Institute of Physics and Technology (State University), 9 Institutskii per., Dolgoprudny, Moscow Region 141701, Russia
[4]Joint Institute for High Temperatures, 13 bd. 2 Izhorskaya St., Moscow 125412, Russia

[a])Electronic mail: sergei.dyachkov@phystech.edu

ABSTRACT

Predictive simulation of the long-term response of multilayer targets with ceramics layers to shock compression demands appropriate material models. Because ceramics are complex brittle materials, which tend to lose their strength under heavy loads, such simulation requires the failure models well-proven for a wide range of strains and strain rates. Standard plate impact experiments provide the main data utilized for developing and validating the mechanical models of material response to shock compression. However, apart from the fact that such experimental data are inherently one-dimensional, they can be insufficient to verify the failure model at relatively low strain rates typical for long unloading waves. Here, we present the experimental results for explosive compression of a spherical multilayer shell initiated by a single detonator. The explosive-coated shell consists of the nested spherical layers: the outer made of boron carbide and the inner of lead. X-ray images showing the evolution of those layers after detonation are then compared with simulation results. Propagation of the compression wave through the layers resulting in ceramics damage is analyzed in detail. We demonstrate that the failure model of boron carbide should be adjusted for compressions below 10 GPa to achieve a good agreement with our experimental images. Such an improved failure model provides the predictive simulation of long-term dynamics of targets after unloading, and it has almost no effect on wave profiles after plate impact.

I. INTRODUCTION

Ceramic materials are known for their unique mechanical strength and high-temperature stability. They have proven to be useful as structural materials in aerospace, nuclear, military, and other industries.[1] Various prototypes containing ceramic parts are being developed. Ceramic layers or microfibers may also be added to composite materials so that those ceramic parts should interact properly with the surrounding media during sound, shock, release, or tensile wave propagation. Thus, a comprehensive material model for ceramics is required to predict their response to various types of loading, including failure process under extreme loads with the formation of cracks and degradation

of their mechanical properties,[2] which complicates development of such a model.

Usually, the fitting parameters of the material model are derived from high-pressure shock Hugoniot data obtained in simple one-dimensional plate impact tests.[3] However, the loading of compound samples containing ceramic parts is mostly three-dimensional, so there is a need for experimental data where a complex composition of waves is formed. Here, we present the experimental x-ray images of the spherical multilayer target containing a boron carbide ceramics layer during its collapse caused by explosive compression initiated at a single point. In such a setup, the boron carbide layer experiences failure at compression induced by the propagation of a

detonation wave, but its unloaded parts keep moving after the end of detonation by inertia, and the boron carbide strength at low pressures reduces the convergence rate of the target.

Underlying atomistic mechanisms related to boron carbide transformations during failure are not completely understood.[4,5] The ballistic experiments[6] demonstrated that the local amorphization bands can be produced under shock compression: they are clearly seen via high-resolution electron microscopy of boron carbide fragments. A similar effect appears at uniaxial compression of boron carbide samples loaded to 50 GPa in diamond anvil cells.[7] The corresponding local structural changes are possibly induced by the C-B-C chain bending, which was demonstrated via quantum molecular dynamics simulation.[7–12] However, this phenomenon is not observed at the hydrostatic loading to 74 GPa.[13]

Shock data[14–21] obtained for various boron carbide materials, having, in particular, the different densities at normal conditions, show the notable variations of the material compressibility under shock loading. The reasons of such shock data variations may include the different grain sizes, stoichiometry, and porosity produced by different manufacturing of samples. However, the idea of the polymorphic phase transition existence near 40 GPa under the application of both high pressure and shear deformation seems to be more appropriate to explain shock data discrepancies, and it is also supported by quantum molecular dynamics simulations.[5]

The only common characteristic in the experimental data is the observed reduction of the boron carbide strength at loads exceeding the Hugoniot Elastic Limit (HEL). This fact is used as a basis for the Johnson–Holmquist approach[3,22] for the simulation of boron carbide ceramics using computational fluid dynamics (CFD) methods. The intact material can be loaded elastically up to a strength limit, the exceeding of which initiates the failure process. During failure, the strength reduces to a lower value with the release of elastic energy resulting in bulking of material. This concept is consistent with the idea of local boron carbide amorphization under compression, which may also have a significant effect on the material strength.

The Johnson–Holmquist failure model was revised recently,[23] where the explicit failure kinetics was introduced. The validation of this explicit failure model on plate impact tests[18,19] revealed the existence of manufacturing dependent properties of boron carbide such as the strength at the failed state. But such plate impact tests are useful to fit the model only at relatively high compressions, because the further behavior of damaged boron carbide after unloading is not available and, thus, cannot be included into the fitting procedure. Here, we perform new simulations using a setup which corresponds our experiment on explosive compression of the spherical multilayer shell. It is found that boron carbide strength parameters should be adjusted in a low pressure range to agree with x-ray images of the shell in dynamics.

Similar to our previous work,[23] we apply the contact smoothed particle hydrodynamics (cSPH) method[24] and use our in-house parallel code[25] CSPH and VD³ to perform simulations using the experimental conditions. The experimental geometry is exactly reproduced in our simulation setup, and the model parameters are adjusted to obtain the proper dynamics of the boron carbide layer after unloading. It should be noted that our aim is to fit both the highly compressed states generated in the plate impact tests[18,19] and the unloaded states of the damaged boron carbide which are essential for long-time evolution observed in our experiment. Such an approach for fitting the failure model is required to cover a wide range of possible scenarios realized in simulations of various engineering prototypes.

II. EXPERIMENT: SETUP AND RESULTS

The experimental multilayer shell consists of four nested spherical layers as shown in Fig. 1:

(1) the plexiglass outer layer (5.9 mm thickness, 57.8 mm outer radius),
(2) the plastic-bonded explosive PBX-9404 layer (11.8 mm thickness, 51.8 mm outer radius),
(3) the boron carbide layer (5 mm thickness, 40 mm outer radius), and
(4) the lead layer (3 mm thickness, 35 mm outer radius).
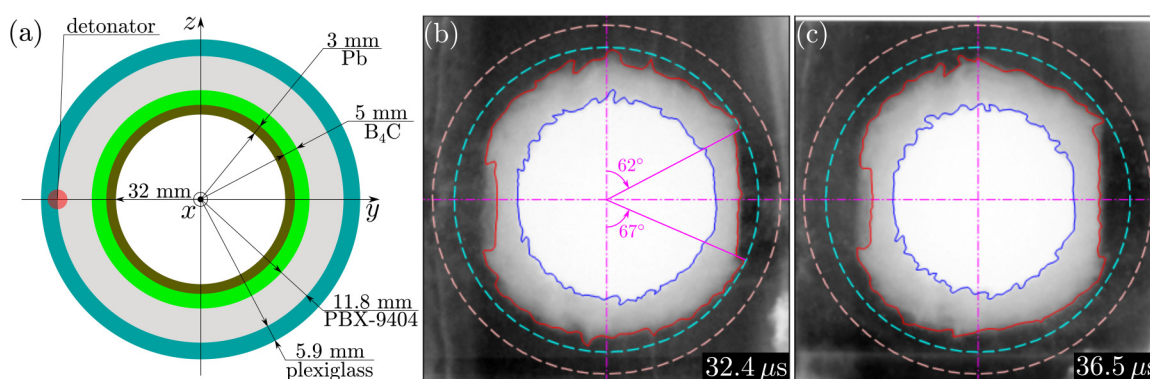
FIG. 1. (a) Sketch of a multilayer shell used in experiments: the nested spherical layers of plexiglass, high explosive material, boron carbide, and lead. A single detonator initiates a detonation wave propagating around the shell. (b) and (c) X-ray images of materials taken along the x-direction at 32.4 μs and 36.5 μs after detonation, respectively. Initial positions of layer boundaries are shown with light red and cyan dashes, while the current positions are marked with red and blue. Perturbations of outer boundaries of the gray-colored boron carbide layer and lead (central white area) are produced by inhomogeneous distribution of damages. A concave is observed in the boron carbide layer at the pole where detonation starts, while another concave is formed around the rear-side pole of the shell.

The detonator is placed at the point of y axis and outer high explosive (HE) layer intersection so that the generated detonation wave first pushes the boron carbide layer from one pole, then propagates around it, and converges at the opposite pole. The lead layer is used to protect the boron carbide layer from unwanted fragmentation from the inside of the layer.

Experimental shadowgraphs were obtained using the two-pulse x-ray facility generating radiation with the boundary energy of ~1 MeV and the half-width pulse duration of ~0.1 μs. The efficient focus of emitter is $f = 2$ mm. X-ray imaging of the prototype is made perpendicular to the symmetry axis passing through the detonator and the center of spherical shell (y axis). Raw images are obtained via photochromic screens ADC-CR. The processed x-ray images of the explosive compression of shell are shown in Fig. 1. Spatial distributions of materials are registered at 32.4 μs and 36.5 μs after detonation, respectively.

The used x-ray is insufficiently hard to reveal the inner surface of the lead layer. Only the outer boundaries of boron carbide and lead layers are observed and traced via the functional method.[26,27] During the experiment, the boron carbide layer is subjected to the nonuniform loading resulting in the material failure at compression. After unloading, the damaged material continues to converge by inertia so that some fragments may be squeezed to the surface forming the observed disturbances. At the pole where detonation is started one can notice a concave on the boron carbide layer, while another concave is produced around the opposite pole.

III. SIMULATION SETUP

A. Model of boron carbide

Because the comprehensive description of the boron carbide model was already given in our recent work,[23] the essential details are merely reproduced here. This model is based on JH-1,[30] JH-2,[3,31] and JHB[32] approaches. The main idea is that the dynamic material strength σ_d is considered as a function of pressure P and damage parameter D: $\sigma_d = \sigma_d(P, D)$. Ceramic material is supposed to harden under compression, but fails if the intact strength limit σ_i is exceeded. Completely damaged material has the lowest strength limit σ_f, and transition from an intact to a failed state during the failure process is described by the simple linear relationship,

$$\sigma_d(P, D) = \sigma_i(P) - D(\sigma_i(P) - \sigma_f(P)), \quad (1)$$

where D is gradually changed from 0 to 1 according to the appropriate failure kinetics.[23]

Johnson et al. proposed to use the following form for the intact and failure strengths as functions of pressure:[22,32]

$$\begin{cases} \sigma_\lambda(P) = \sigma_\lambda^0 + (\sigma_\lambda^{\max} - \sigma_\lambda^0)\{1 - \exp[-\alpha_\lambda(P - P_\lambda^0)]\}, & P > P_\lambda^0, \\ \sigma_\lambda(P) = \sigma_\lambda^0(P + T_\lambda)/(P_\lambda^0 + T_\lambda), & P < P_\lambda^0, \end{cases} \quad (2)$$

with

$$\alpha_\lambda = \sigma_\lambda^0 / [(\sigma_\lambda^{\max} - \sigma_\lambda^0)(P_\lambda^0 + T_\lambda)], \quad (3)$$
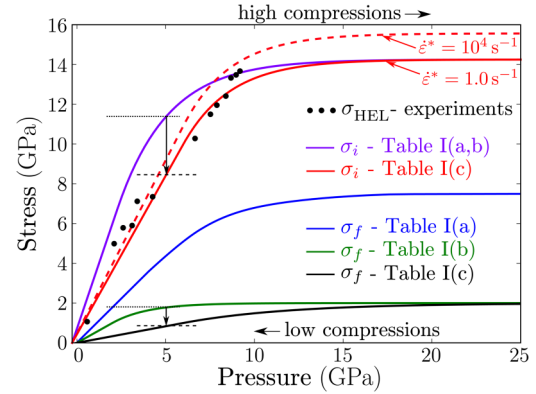

FIG. 2. Boron carbide strength limits $\sigma_i(P)$ and $\sigma_f(P)$ used in earlier work[23] and the modified ones. According to Holmquist and Johnson,[22] the elastic shock-wave data[19,28,29] presented here correspond to the intact strength limit. Correction of σ_i and σ_f limits is required to reduce the strength at low pressures, what schematically shown by arrows at $P = 5$ GPa. The new slope of $\sigma_i(P)$ is in a better agreement with the experimental values for σ_{HEL}. Though, such a change provides almost no effect on wave profiles simulated according to plate impact tests, it makes easier deformation of partly damaged boron carbide layer after explosive compression.

where $\lambda = i, f$ is either for the intact or for the failed material. The strength limit is supposed to depend on the strain rate,

$$\sigma_\lambda(P, \dot{\varepsilon}^*) = \sigma_\lambda(P)(1 + C \ln \dot{\varepsilon}^*), \quad (4)$$

where $\dot{\varepsilon}^* = \dot{\varepsilon}_e / \dot{\varepsilon}_0$ is the dimensionless strain rate obtained by the rate divider $\dot{\varepsilon}_0 = 1.0\, \mathrm{s}^{-1}$, $\dot{\varepsilon}_e$ is the equivalent strain rate, and C is a constant. Typical curves are shown in Fig. 2.

The appropriate sets of parameters $\{\sigma_i^0, \sigma_i^{\max}, P_i^0\}$ and $\{\sigma_f^0, \sigma_f^{\max}, P_f^0\}$ were adjusted earlier[3,22,23] for two different plate impact tests performed by Grady and Moody[18] and Vogler et al.[19] The parameters fitted to reproduce the "hard" ceramics used in Vogler's test are listed in the column (a) of Table I, while the parameters for "soft" ceramics in Grady's tests are in the column (b).

It was noticed that the different types of boron carbide used in those tests were manufactured using the different technologies, which may be a reason for their different behavior.[22] It was

TABLE I. Parameters of strength limits $\sigma_i(P)$ and $\sigma_f(P)$ for (a) "hard" and (b) "soft" types of boron carbide.[3,22,23] The newly adjusted parameters are in (c).

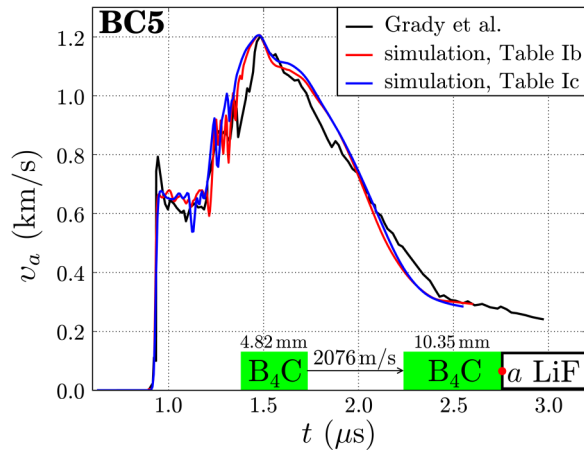| Parameter (GPa)	(a)	(b)	(c)
Intact strength, σ_i^0	6.7	6.7	10.0
Intact strength, $\sigma_i^{\max}$	14.3	14.3	14.3
Intact strength, P_i^0	2.3	2.3	6.0
Failure strength, σ_f^0	5.0	1.0	1.0
Failure strength, $\sigma_f^{\max}$	8.5	2.0	2.0
Failure strength, P_f^0	5.0	2.0	6.0

FIG. 3. Simulated and experimental interface velocities for the BC5 test[18] using boron carbide strength parameters from our previous paper[23] and after new adjustment, see the corresponding columns (b) and (c) in Table I. The target/LiF window interfaces are marked by "a." One can notice that the obtained profiles are almost identical.

quantitatively demonstrated[23] that the difference between two experiments can be described barely by varying the upper limit $\sigma_f^{\max}$ of σ_f function. Similarly, the amplitude of the elastic precursor is defined by the upper limit $\sigma_i^{\max}$ of σ_i function. Variations in other parameters, which are responsible for the slope of σ_i and σ_f at low pressures, are of no significance in simulations of plate impact tests and thus cannot be fitted properly.

Nevertheless, the changes in slopes of the σ_i and σ_f curves at low pressures, which are defined by σ_λ^0 and P_λ^0, $\lambda = i, f$, may take a significant effect on the strength properties of boron carbide. But the reduction of strength by $2-3$ GPa at the low compressions can be achieved without affecting the highly compressed states, as shown in Fig. 2. Such adjustments of the slopes of the strength curves make easier deformation of the boron carbide layer under lower stresses, which has a significant effect on long-term convergence dynamics of the shell as demonstrated below in Sec. IV B.

The adjustment of failure model parameters, which provides a new set of parameters listed in Table I(c), is discussed below in Sec. IV C. We performed simulations of the BC5 plate impact experiment[18] using those new parameters and found that these changes in slope of $\sigma_i(P)$ below 10 GPa from the columns (b) and (c) in Table I take almost no effect on the wave profiles, as illustrated in Fig. 3. That is why the validation of failure model should include experiments in which the long-term evolution of targets is mostly guided by inertia and low stresses.

B. Model of high explosive

The detonation of the plastic-bonded explosive PBX-9404 is simulated using the macrokinetics rate equation and the Johnson–Wilkins–Lee (JWL) equation of state.[33] The "ignition and growth model" for the mass fraction λ of products in explosive transformation

provides the rate equation,

$$\frac{d\lambda}{dt} = -I(1-\lambda)^{2/9}\left(\frac{v_{0s}}{v_s} - 1\right)^4 - J(1-\lambda)^{2/9}\lambda^{2/9}P^Z, \quad (5)$$

where subscript s stands for the solid phase, $v_s = 1/\rho_s$ is the current specific volume of the solid phase, $v_{0s} = 1/\rho_{0s}$ is the initial specific volume of the solid phase.

The following constants for PBX-9404 are used in the simulation: $I = 44 \mu s^{-1}$, $J = 0.126 \mu s^{-1}$ GPa^{-Z}, and $Z = 1.6$. The rate equation (5) is consistent with the JWL equation of state described in the following.

The equation of state for the unreacted explosive and products is given by

$$\frac{E_s}{v_{s0}} = \frac{P_s \tilde{v}_s}{\omega_s} - F_s(\tilde{v}_s) + F_s(1), \quad (6)$$

$$\frac{E_g}{v_{s0}} = \frac{P_g \tilde{v}_g}{\omega_g} - F_g(\tilde{v}_g) - Q, \quad (7)$$

whose thermal equation of state is

$$P_s = \frac{\omega_s}{\tilde{v}_s}\left[C_s T_s + G(\tilde{v}_s) + F_s(\tilde{v}_s)\right], \quad (8)$$

$$P_g = \frac{\omega_g}{\tilde{v}_g}\left[C_g T_g + G(\tilde{v}_g) + F_g(\tilde{v}_g)\right], \quad (9)$$

and additive relations for the internal energy E and specific volume v as

$$v = (1-\lambda)v_s + \lambda v_g, \quad (10)$$

$$E = (1-\lambda)E_s + \lambda E_g, \quad (11)$$

and the thermodynamic equilibrium conditions for pressure P and temperature T,

$$P_s = P_g = P, \quad (12)$$

$$T_s = T_g = T. \quad (13)$$

Equations (6)–(9) utilize the following functions:

$$F_i(\tilde{v}_i) = A_i\left(\frac{\tilde{v}_i}{\omega_i} - \frac{1}{R_{1i}}\right)e^{-R_{1i}\tilde{v}_i}$$
$$+ B_i\left(\frac{\tilde{v}_i}{\omega_i} - \frac{1}{R_{2i}}\right)e^{-R_{2i}\tilde{v}_i},$$

$$G_i(\tilde{v}_i) = \frac{A_i}{R_{1i}}e^{-R_{1i}\tilde{v}_i} + \frac{B_i}{R_{2i}}e^{-R_{2i}\tilde{v}_i},$$

where $\tilde{v}_i = v_i/v_{s0}$, $i = s, g$ are for the solid and gaseous phases, respectively.

TABLE II. PBX-9404 parameters.

Parameter	Solid phase (s)	Gaseous phase (g)
ρ_0 (kg/m^3)	1842	…
Q (MJ/kg)	…	5.39
A (GPa)	6969	852.4
B (GPa)	-172.7	18.02
R_1	7.8	4.6
R_2	3.9	1.3
ω	0.8578	0.38
C_v (J/g/K)	1.360	0.571
Chapman–Jouguet parameters		
c_{CJ} (km/s)	6502	
P_{CJ} (GPa)	36.78	
D_{CJ} (km/s)	8.78	

TABLE III. Parameters of plexiglass and lead.

Parameter	Lead	Plexiglass
ρ_0 (g/cm^3)	11.35	1.19
c (km/s)	2.58	3.5
s	1.26	1.15
γ	1.7	0.97

With the given λ, v, E, the unknown quantities in Eqs. (6)–(13) are

$$v_s, v_g, T_s, T_g, P_s, P_g, E_s, E_g.$$

HE constants are given in Table II. A linear relationship between shock and mass velocity $u_s = c_i + s_i u_p$ is used, where c_i is the bulk sound speeds and s_i is the fitting parameters for $i = s, g$, which are required to obtain the Riemann solution using the Dukowicz solver.[34] In particles with $0 < \lambda < 1$, these parameters are mixed as follows:

$$c^2 = \lambda c_g^2 + (1 - \lambda)c_s^2, \tag{14}$$

$$s = \lambda s_g + (1 - \lambda)s_s. \tag{15}$$

The shock Hugoniot equation of unreacted explosive is obtained and solved numerically as[35]

$$\tilde{v}_s{}^2 - 2\left(\frac{1 + \omega_s}{2 + \omega_s}\right)\tilde{v}_s + \frac{\omega_s}{2 + \omega_s}$$
$$- 2\left(\frac{2\omega_s}{2 + \omega_s}\right)\frac{v_{s0}}{u_s^2}[F_s(1) - F_s(\tilde{v}_s)] = 0. \tag{16}$$

The dependence of u_s on u_p follows from the solution of Eq. (16) and mass flow equation providing $c_s = 2319\,\text{m/s}$, $s_s = 1.447$. Coefficients for products are $c_g = c_{CJ}$, where c_{CJ} is the Chapman–Jouguet sound velocity and $s_g = (\omega_g + 2)/2$.

C. Lead and plexiglass models

The equations of state for plexiglass and lead are in the Mie–Grüneisen form,

$$P = P(\rho, e) = P_r + \Gamma\rho(e - e_r). \tag{17}$$

The reference pressure P_r and internal energy e_r are obtained using a linear approximation $u_s = c + s u_p$ of the shock velocity u_s from the material velocity u_p, where c is a bulk sound velocity in an

uncompressed material and s is a fitting parameter. By denoting $x = 1/\delta = \rho_0/\rho$, the reference pressure and energy as functions of density can be expressed as follows:

$$P_r(\rho) = \rho_0 c^2 \frac{1 - x}{[1 - s(1 - x)]^2}, \quad e_r = \frac{P_r}{\rho_0}\frac{(1 - x)}{2}, \tag{18}$$

where $x = \rho_0/\rho$ is the compression ratio. The used parameters for the equation of states of plexiglass and lead are given in Table III. Strength properties of lead and plexiglass are not taken into account because they are much smaller than those of boron carbide.

D. Simulation technique

Explosive compression of shell is simulated using the smoothed particle hydrodynamics (SPH) method, where the Riemann problem solution is applied at interparticle contacts.[24] This meshless Lagrangian method is also referred to as the contact SPH (cSPH) method and seems to be most suitable for simulations of shock propagation which is followed by material failure and fragmentation: the formation of complex voids, cracks, and free boundaries is simulated naturally using SPH, while the grid-based methods require special algorithms to handle these phenomena. The details of cSPH related to simulation of ceramics are covered comprehensively in our recent paper.[23]

The advantage of SPH is an opportunity to set up an arbitrary distribution of particles with the only requirement,

$$\sum_j \frac{m_j}{\rho_j} W(r_{ij}, h) \simeq 1, \tag{19}$$

where $W(r, h)$ is the smoothing kernel with the smoothing length h, ρ_j is the density of particle j, m_j is the mass of particle j, and r_{ij} is the distance between particles i and j. The most simple way to set up particles is to place them using a regular lattice. However, the nested spherical layers of shell will have the stepped boundaries in such case. These boundary perturbations may lead to nonphysical results, so that a special algorithm is applied to eliminate the step-induced effects. Initially, the random forces are applied to move interior particles in the bulk of sample, while the boundary particles are pushed inward along normal vectors. After that, a high pressure is applied to particles in the bulk to achieve the condition (19), which results in a liquidlike particle distribution in samples with smooth boundaries.

To take advantage of the cSPH method, a good spatial resolution is required. In our simulations, the initial size of SPH particle is set to 0.2 mm so that the complete setup shown in Fig. 1(a) involves about 58 million particles. Simulation is performed using

our in-house 3D SPH code with the efficient parallel load balancing algorithm based on dynamical domain decomposition of samples between Voronoi subdomains.[25] Particles within each Voronoi subdomain are handled by a separate MPI process which is performed on a single processor core. During a simulation, the load balancing algorithm shifts the less loaded Voronoi subdomains toward their heavy loaded neighbors. As a result, the particles are redistributed between processes leading to reduction of wasted times for waiting of intercore communications.

It is found that unloading of the gaseous products of high explosive to pressures below 1 GPa occurs quite fast, so these gas-phase particles may be removed without affecting the dynamics of boron carbide and lead layers. Thus, the most particles required to simulate outer layers of HE and plexiglass can be removed after expansion what releases computational resources for the inner layers. A complete simulation (up to $100\,\mu s$) takes about 10 h of operation using 512 processor cores of cluster with Intel Xeon E5-2670.

IV. SIMULATION RESULTS

A. Analysis of wave propagation

The analysis of wave propagation induced by the HE detonation is based on the simulation using the boron carbide strength properties listed in Table I(c). Though the strength variations in the boron carbide model will be shown to have a noticeable effect on the later stages of shell dynamics, the early stage, when the detonation wave produced at one pole encompasses the spherical shell and converges at the opposite pole, is quite the same.

The results of simulations are convenient to observe using the 5 mm width meridian slice of a sphere which contains the y axis of symmetry as shown in Fig. 4 (Multimedia view). There are two-dimensional color maps for each slice averaged over its width, and the colors correspond to the following material properties: the density for plexiglass and lead (denser material is darker), the pressure for HE, and the damage parameter for boron carbide (light green for the intact and black for the failed material). These color maps are found to suit best for illustration, however the quantitative analysis requires an additional type of data representation. In Fig. 4 (Multimedia view), one can notice that by the moment when the detonation wave approaches the second pole, the boron carbide and lead shells have small deformation of their spherical shape. Thus, the angular pressure profiles are representative enough to demonstrate the main features of wave propagation within materials. For each material, the quantities such as pressure and equivalent stress are averaged along the angular direction with a $0.5°$ step providing the corresponding angular profiles for the considered slice of a sphere.

The early stage of explosive compression is split into six steps marked with letters (a, b, c, d, e, f) in Fig. 4 (Multimedia view). In the beginning shown in Fig. 4(a) (Multimedia view), the detonator induces the expanding spherical detonation wave which compresses the boron carbide layer producing the intense damage in the front pole. It is followed by the short pressure relaxation near the pole after which the main detonation wave begins to encircle the spherical layer. Figure 4(b) (Multimedia view) shows that the failure front in boron carbide is ahead of the detonation front: the sliding detonation pushes the boron carbide layer around the detonation front so that the wave of the semitriangular shape is produced forward due to

high sound speed of boron carbide. The wave splits into the pure elastic and failure waves at the position where the intact strength is exceeded. The elastic wave encircles the boron carbide layer much faster, and by the moment when the main detonation wave reaches the equator [Fig. 4(c)] (Multimedia view), it converges to the opposite pole and begins to combine itself with the fast stress and pressure growth. A few moments later, the elastic compression of boron carbide around the rear-side pole reaches the extreme pressures as shown in Fig. 4(d) (Multimedia view) so that the material fails producing several failure bands just before arrival of the main detonation and failure waves [Fig. 4(e)] (Multimedia view). It is interesting that such pressure focusing in boron carbide around the rear-side pole results in unloading into the neighboring lead and HE layers, which produces pressures high enough to initiate an additional rear-side detonation wave colliding later with the arriving main detonation wave as shown in Fig. 4(f) (Multimedia view).

The early stage is assumed to be completed when the main detonation wave converges at the rear pole producing the last pressure pulse backwards, so that the further dynamics proceeding by inertia is guided by low internal stresses in the later stage. Thus, during inertial convergence, the boron carbide layer is under deformation producing the internal stress which slows down its further deformation. Moreover, the greater induced stress obtained from the used failure model, the slower deformation and convergence of boron carbide layer should be observed in simulation. Figure 4 (Multimedia view) shows that the equivalent stress and pressure are about 3–6 GPa what identifies the pressure range where the failure model parameters should be accurately adjusted.

B. Effect of the failed strength limit

Johnson and Holmquist had noted[22] that the boron carbide samples manufactured in different ways may provide rather different wave profiles in BC-10[18] and BC-X[19] tests used in similar experimental setups. The underlying mechanics of that was associated[23] with variations of strength limit $\sigma_f(P)$ in the failed ceramics. Being fitted to reproduce properly the Vogler et al.[19] tests, the explicit failure model of boron carbide was found to have the smaller limit σ_f to fulfil the description of the Grady et al. tests.[18] However, the suggested changes in $\sigma_f(P)$ were validated only for plate impact tests providing data at high compressions mostly, but additional adjustment and validation are required for low compressions.

To test the effect of the strength limit on the late shell dynamics, we performed additional simulations using parameters listed in Tables I(a) and I(b). The results are represented by color maps in Fig. 5, similar to the ones used in Fig. 4 (Multimedia view), but with HE and plexiglass hidden. In addition, the experimental outer boundaries of boron carbide and lead layers, which are shown in Figs. 1(b) and 1(c) for the times of $32.37\,\mu s$ and $36.47\,\mu s$ after detonation, respectively, are mapped in Fig. 5 using red and cyan colors. Color maps denoted with (a) and (b) in the top of Fig. 5 correspond the boron carbide with parameters from Table I(a) for "hard" ceramics, while (c) and (d) in the middle are obtained using parameters from Table I(b) for "soft" ceramics.

First of all, the analysis of Fig. 5 demonstrates that the simulated outer boundary of the lead layer fits the experimental result very well for the both "soft" and "hard" types of the failed boron
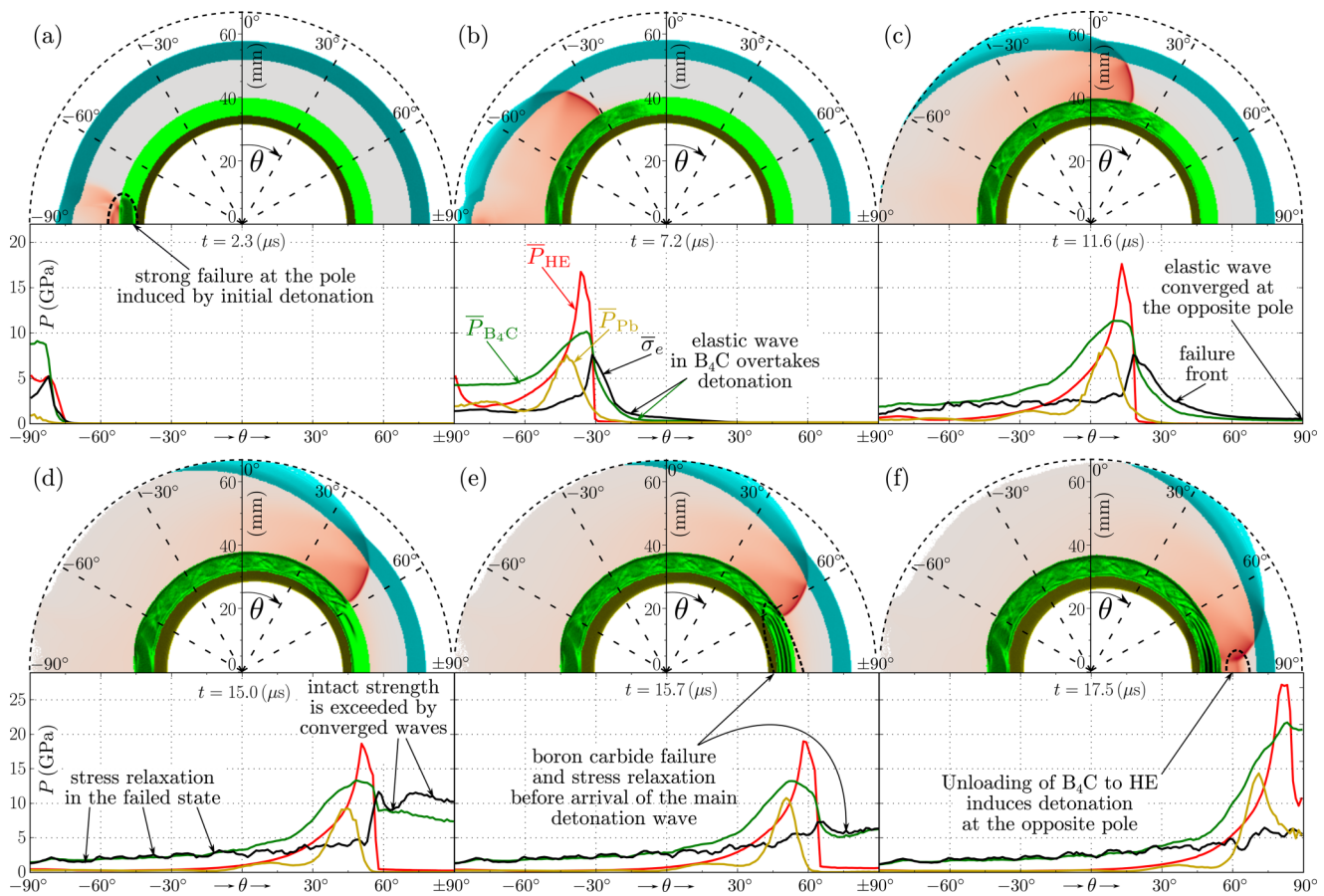
FIG. 4. Propagation of waves is shown both in color maps and angular profiles. The quantities $\overline{P}_{HE}$ is the pressure in high explosive, $\overline{P}_{Pb}$ is the pressure in lead, $\overline{P}_{B_4C}$, $\overline{\sigma}_e$ is the pressure and the equivalent stress in boron carbide are averaged along the angular direction with $0.5°$ step. (a) The detonation wave propagates to the boron carbide shell and induces strong failure at its first pole. (b) Detonation develops and encompasses the boron carbide shell so that the pressure in the HE material P_{HE} compresses B_4C leading to its failure, however, the elastic wave in B_4C propagates much faster and is ahead of the detonation and failure waves. (c) By the moment the detonation and failure waves have propagated to the equator, the elastic wave in B_4C has reached the second pole. (d) The elastic wave in B_4C converges at the second pole resulting in the extreme stress, while behind the failure front the stress is relaxed. (e) The extreme stress at the second pole induces the abrupt failure of boron carbide with several layers of failure bands and stress relaxation, while the main failure and detonation waves are still approaching. (f) The elastically compressed boron carbide at the second pole unloads to the HE shell what induces its detonation while the main detonation wave is still approaching. The complete simulation is shown in the corresponding Supplement Movie. Multimedia view: https://doi.org/10.1063/1.5099013

carbide. However, the boron carbide layer behaves rather different depending on the used σ_f. In fact, both types of ceramic layers appear to be too hard to converge and fit the layer boundaries obtained in the experiment. A positive tendency is that the "soft" type of the failed boron carbide seems to converge faster than the "hard" one. As soon as a lot of material is still undamaged (the damage parameter $D \sim 0$) which is marked with the light green color, the strength of intact ceramics at low compressions should have a noticeable effect on the shell convergence rate.

C. Adjusting boron carbide strength properties

Because the slower convergence of the simulated shell is associated with the large part of remaining undamaged boron carbide,

the strength limit of intact ceramics should be reduced to fit the experiment. It is obvious from Fig. 2 that our previous fit[23] for $\sigma_i(P)$ overestimates the experimental values for σ_{HEL} listed in the Johnson and Holmquist's work,[22] but the usage of this fit does not provide any noticeable effect on simulated plate impact tests which agree well with the experiments. The reason is that at high compressions, which are usually achieved after a high velocity impact, σ_i^{max} plays a key role, while the initial slope of the intact curve $\sigma_i(P)$ may vary without visible consequences in the simulated wave profile. The only requirement here is that this slope must not exceed one of the elastic loading path 0 shown in Fig. 2 in our previous paper.[23] Otherwise, the elastic loading may reach the intact strength limit much earlier what results in a too weak elastic precursor.
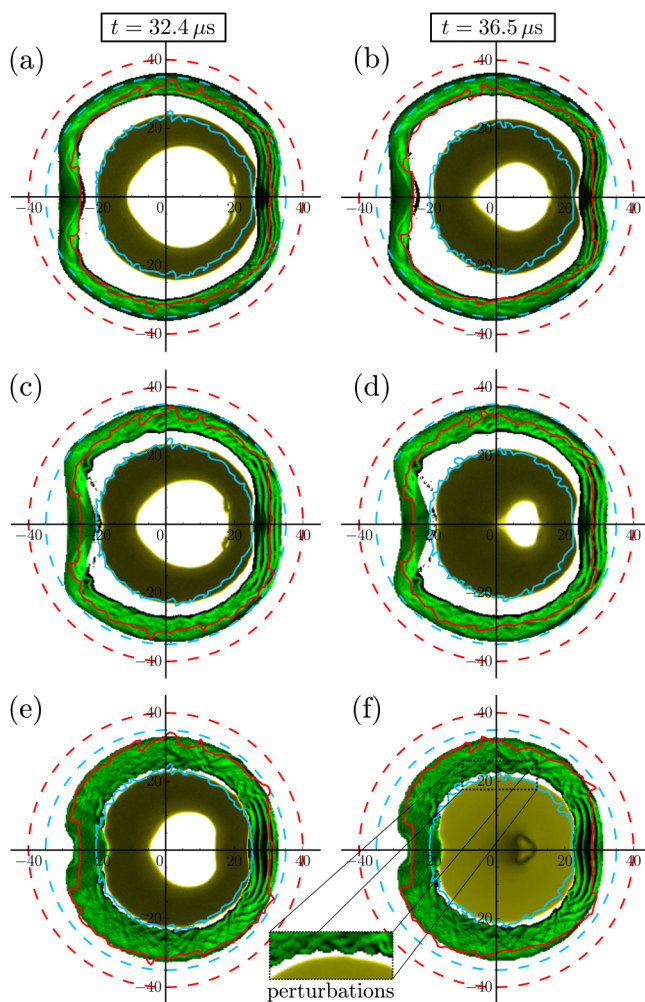
FIG. 5. Simulations with different strength parameters of boron carbide are compared to the experiment. Red and cyan dashes represent the initial outer boundaries of B$_4$C and lead layers, while solid lines define their current positions in the experiment. Color of the boron carbide layer represents its damage parameter D changing from 0 (light green, undamaged) to 1 (black, failed). Color of the lead layer represents its density so that the darker material is more dense. (a) and (b) Simulation with parameters from Table I(a). (c) and (d) Simulation with parameters from Table I(b). Strength limit of the failed ceramics is low in this case, so the overestimated strength, which keeps the layer from necessary convergence, should be due to large amount of the undamaged material. (e) and (f) Simulation with parameters from Table I(c). Change in the slope of the intact strength $\sigma_i(P)$ at low compressions lead to the necessary position of the outer boundary of the boron carbide layer.

Following the aforementioned suggestions, a simulation is performed using the newly adjusted boron carbide parameters listed in Table I(c) which provide a less steeper initial slope of $\sigma_i(P)$. Figure 2 shows that this part of the intact strength curve now agrees well with the experimental stress σ_{HEL} in the elastic precursor and provides a much lower strength limit at compressions

about 5 GPa. To "soften" boron carbide even more, the strength limit of failed ceramics $\sigma_f(P)$ is also reduced for that range of compressions.

The simulation results are compared to the experiment in Figs. 5(e) and 5(f). The performed adjustments allow the boron carbide layer to converge much farther, so it fits the outer boundary of the experimental one quite well. At the pole, where detonation is initiated, one can observe the formation of a concave that agrees with the experiment. The outer boundary of the lead layer in this simulation still fits the experimental one with the following difference: the concave at the pole from the outside of B$_4$C layer produces a hill inside pushing the lead layer. This deformation appears at the pole forming a cavity which may be hidden in x-ray images as well as the inner cavity.

The visible flattening of boron carbide layer leading to another concave around the opposite pole, which is observed in the experiment, is not reproduced in our simulations precisely. However, an explanation of the observed phenomenon follows from the late stages of wave propagation shown in Figs. 4(d)–4(f) (Multimedia view). The part of boron carbide layer localized around the rear pole experiences abrupt strength degradation due to elastic wave convergence resulting in the formation of several stripes of failure bands. This part is more yieldable for deformation than less damaged ones. The arrived detonation wave plus the secondary detonation around the rear-side pole deforms this part of boron carbide layer forming the rear-side concave. Our simulation shows that failure bands spread around the opposite pole starting at about 62°, which happens at about 15 μs as shown in Fig. 4(e) (Multimedia view). This angle agrees well with the onset of rear-side concave in the range of 62°−68° obtained in the experiment, see Fig. 1(b).

Another interesting observation from the last simulation is that the inner surface of converged boron carbide layer becomes perturbed due to inhomogeneous distribution of damages localized mostly in the failure bands. If there was a contact between boron carbide and lead layers, the latter would be perturbed as well, and that seems to be happened in the experiment, see Fig. 1.

It is also worth noting that the resistance of the boron carbide layer to strain in the experiment is lower than one in our simulations possibly due to inhomogeneous density of the used ceramics. The experimental sample has the density variations in the range of 2.35−2.55 g/cm^3. We expect that such a sample should have higher strain under similar load leading to the increased stress and larger amount of the failed material. As a result, the boron carbide layer should converge even farther. But the model with such density variations will be inconsistent with uniaxial shock data,[18,19] where the density of boron carbide is close to one of the monocrystals for which the current model is developed. The agreement can be achieved here for low compressions, but an additional set of uniaxial tests is required to verify the boron carbide model with the density inhomogeneity at high compressions. Within the framework of the current model, only strength properties of boron carbide can be adjusted.

D. Further evolution and fragmentation of shell

Our aim to adjust boron carbide properties using the new experimental data is attained in Secs. IV A–IV C, but it is
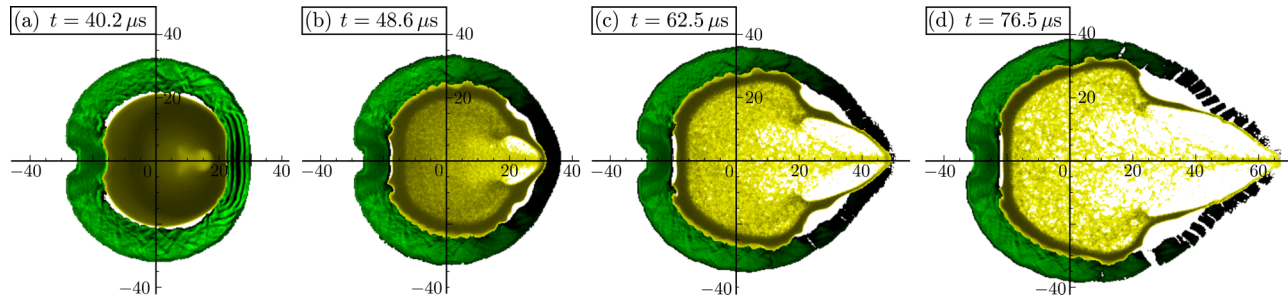
FIG. 6. Formation of lead jet, cavitation in lead, and fragmentation of the boron carbide layer: (a) the part of the lead layer which is closer to the detonator has greater velocity so that the asymmetric convergence of the lead layer to the shell center occurs resulting in the formation of a cumulative jet; (b) the diverging shock wave is formed after collapse of the lead layer leading to its expansion with further cavitation induced by the tensile stress exceeding of tensile strength; (c) the expansion distributes lead around the boron carbide layer from inside, while the jet breaks the boron carbide layer; (d) debris is formed around the jet as it penetrates through the boron carbide.

interesting to trace the further evolution of boron carbide and lead layers. It may be used to plan further experiments focused on other characteristics such as spall strength or fragment size distribution, which may be utilized in an extended failure model.

Figure 6 shows the late stage evolution continued from Fig. 5, where boron carbide is simulated with the strength parameters listed in Table I(c). The detonation wave started at the left pole produces the converging shock wave penetrating in the boron carbide and lead layers. Such asymmetric loading results in asymmetric material flow toward the shell center where the left part of lead layer converges faster than the rear-side part, see the movie linked to Fig. 4 (Multimedia view). This convergence of material at the center causes a pressure jump up to ∼130 GPa at a focal point, which generates a new diverging shock wave. This produces an ejecta directed to the remaining part of central cavity. Thus, a cumulative lead jet is formed with velocity directed toward the opposite rear-side pole.

The shock wave diverging from the focal point accelerates material outward, which results in the formation of tensile stress in lead. The cavitation process observed in the bulk of stretched lead near the center looks realistic, see Fig. 6, but we assume that the tensile strength is fixed at 1 GPa in this particular simulation. Usually, the proper relation between the tensile strength and strain rate is required for simulations of this kind,[36] but being focused on boron carbide properties, we used a simplified cavitation model for lead here.

The diverging shock wave hits the surrounding boron carbide layer, stops its contraction, and initiates expansion. Later, the most part of expanding lead reaches the boron carbide layer inducing its further expansion, while the cumulative jet develops and interacts with it at the rear pole. Ceramics around the rear pole fails completely during interaction with the jet because the tensile strength T tends to zero in the used failure model.[23] Thus, the farther propagation of the jet meets almost no resistance resulting in fragmentation with the formation of boron carbide debris around the rear pole.

V. CONCLUSION

Large-scale predictive simulation of complex samples having boron carbide parts requires a material model which must be applicable in a wide range of conditions. One-dimensional plate impact tests are the main data source for retrieving the model parameters at high compressions, but the long-term dynamics of almost unloaded samples at lower stresses may be reproduced incorrectly using those parameters. In this work, we report the experimental dynamics of the multilayer shell with the boron carbide layer under explosive compression initiated by a single point detonator. At the stages captured in x-ray images, the detonation of a high explosive layer covering the shell is finished, and the boron carbide layer moves by inertia. Thus, its movement is guided by strength parameters at low compressions, which can be obtained from several probing simulations.

The simulations performed using the cSPH method with high 3D spatial resolution demonstrate that the strength properties of boron carbide unloaded below 10 GPa have a considerable effect on the shell convergence dynamics. However, it is found that variations of the strength limit σ_f in failed ceramics of different types cannot itself explain the inconsistency between the presented simulation and experiment. Instead, the slope of the intact ceramics strength σ_i at low compressions is shown to be a key to the final agreement. Moreover, a smaller slope of $\sigma_i(P)$ below 10 GPa gets us closer to values of σ_{HEL} collected by Johnson and Holmquist.[22] Such an effect of σ_i is almost impossible to take into account using only wave profiles from plate impact tests: they are shown to remain unchanged after our modifications to strength properties at low pressures.

Apart from the improvements made to the boron carbide failure model using our experimental data, we have analyzed the process of wave propagation through the shell in detail. An interesting phenomenon is observed around the pole opposite to the detonator location: having the high sound speed boron carbide becomes elastically loaded enough to fail abruptly near the rear-side pole before the arrival of the main detonation wave. Such a change in material properties allows the external compression to form a concave of a special shape within the boron carbide layer around the rear-side pole as observed in the experiment. However, we did not come to an exact agreement between simulation and the experiment about such indenting, what may be due to a smaller density of experimental boron carbide. Nevertheless, the shape of

the boron carbide layer around the rear-side pole definitely changes under explosive compression in all our simulations. In addition, elastic loading of the boron carbide to its HEL is enough to initiate a second detonation within the adjacent layer of high explosive before the main detonation wave arrives to the rear-side pole.

Finally, we have observed the formation of ejecta after the asymmetrical convergence of lead layer and expansion of lead resulting in its cavitation nearby the shell center. While the most part of lead reaches the boron carbide layer and push it out, the lead jet breaks the boron carbide layer from the inside around the rear-side pole forming a cloud of fragments. Their size distribution may be compared with experimental ones if the further improvement of failure model will be implemented.

ACKNOWLEDGMENTS

REFERENCES

[1]I. Low, "Advances in ceramic matrix composites: An introduction," in *Advances in Ceramic Matrix Composites*, edited by I. Low (Woodhead Publishing, 2014), pp. 1–6.

[2]D. E. Grady, "Shock-wave compression of brittle solids," Mech. Mater. **29**, 181–203 (1998).

[3]G. R. Johnson and T. J. Holmquist, "Response of boron carbide subjected to large strains, high strain rates, and high pressures," J. Appl. Phys. **85**, 8060–8073 (1999).

[4]V. Domnich, S. Reynaud, R. A. Haber, and M. Chhowalla, "Boron carbide: Structure, properties, and stability under stress," J. Am. Ceram. Soc. **94**, 3605–3628 (2011).

[5]D. E. Grady, "Hugoniot equation of state and dynamic strength of boron carbide," J. Appl. Phys. **117**, 165904 (2015).

[6]M. Chen, J. W. McCauley, and K. J. Hemker, "Shock-induced localized amorphization in boron carbide," Science **299**, 1563–1566 (2003).

[7]X. Q. Yan, Z. Tang, L. Zhang, J. J. Guo, C. Q. Jin, Y. Zhang, T. Goto, J. W. McCauley, and M. W. Chen, "Depressurization amorphization of single-crystal boron carbide," Phys. Rev. Lett. **102**, 075505 (2009).

[8]S. Aryal, P. Rulis, and W. Y. Ching, "Mechanism for amorphization of boron carbide B_4C under uniaxial compression," Phys. Rev. B **84**, 184112 (2011).

[9]Q. An, W. A. Goddard, and T. Cheng, "Atomistic explanation of shear-induced amorphous band formation in boron carbide," Phys. Rev. Lett. **113**, 095501 (2014).

[10]D. E. Taylor, "Shock compression of boron carbide: A quantum mechanical analysis," J. Am. Ceram. Soc. **98**, 3308–3318 (2015).

[11]P. Korotaev, P. Pokatashkin, and A. Yanilkin, "Structural phase transitions in boron carbide under stress," Model. Simul. Mater. Sci. Eng. **24**, 015004 (2016).

[12]P. Korotaev, P. Pokatashkin, and A. Yanilkin, "The role of non-hydrostatic stresses in phase transitions in boron carbide," Comput. Mater. Sci. **121**, 106–112 (2016).

[13]P. Dera, M. H. Manghnani, A. Hushur, Y. Hu, and S. Tkachev, "New insights into the enigma of boron carbide inverse molecular behavior," J. Solid State Chem. **215**, 85–93 (2014).

[14]M. L. Wilkins, Third progress report of light armor program, Technical Report UCRL50460, Lawrence Livermore National Laboratory, University of California, CA, 1968.

[15]W. H. Gust and E. B. Royce, "Dynamic yield strengths of B_4C, BeO, and Al_2O_3 ceramics," J. Appl. Phys. **42**, 276–295 (1971).

[16]M. N. Pavlovskii, "Shock compressibility of six very hard substances," Sov. Phys. Solid State **12**, 1736–1737 (1971).

[17]*LASL Shock Hugoniot Data*, edited by S. P. Marsh (University of California Press, Berkley, 1980), p. 657.

[18]D. E. Grady and R. L. Moody, Shock compression profiles in ceramics, Technical Report SAND96-0551, Sandia National Laboratories, 1996.

[19]T. J. Vogler, W. D. Reinhart, and L. C. Chhabildas, "Dynamic behavior of boron carbide," J. Appl. Phys. **95**, 4173–4183 (2004).

[20]Y. Zhang, T. Mashimo, Y. Uemura, M. Uchino, M. Kodama, K. Shibata, K. Fukuoka, M. Kikuchi, T. Kobayashi, and T. Sekine, "Shock compression behaviors of boron carbide (B_4C)," J. Appl. Phys. **100**, 113536 (2006).

[21]G. I. Kanel, E. B. Zaretsky, A. M. Rajendran, S. V. Razorenov, A. S. Savinykh, and V. Paris, "Search for conditions of compressive fracture of hard brittle ceramics at impact loading," Int. J. Plast. **25**, 649–670 (2009).

[22]T. J. Holmquist and G. R. Johnson, "Characterization and evaluation of boron carbide for plate-impact conditions," J. Appl. Phys. **100**, 093525 (2006).

[23]S. A. Dyachkov, A. N. Parshikov, M. S. Egorova, S. Y. Grigoryev, V. V. Zhakhovsky, and S. A. Medin, "Explicit failure model for boron carbide ceramics under shock loading," J. Appl. Phys. **124**, 085902 (2018).

[24]A. N. Parshikov and S. A. Medin, "Smoothed particle hydrodynamics using interparticle contact algorithms," J. Comput. Phys. **180**, 358–382 (2002).

[25]M. S. Egorova, S. A. Dyachkov, A. N. Parshikov, and V. V. Zhakhovsky, "Parallel SPH modeling using dynamic domain decomposition and load balancing displacement of Voronoi subdomains," Comput. Phys. Commun. **234**, 112–125 (2019).

[26]V. A. Arinin, "Functional method of tracing of demarcations of two mediums having cylindrical geometry," in *Digital Signal Processing and Its Applications—2006 (DSPA-2006)* (AUTEX Spb., 2006), pp. 457–460 (in Russian); available at http://www.autex.spb.su/download/dsp/dspa/dspa2006/t2/2-34.pdf

[27]V. A. Arinin and B. I. Tkachenko, "Achieving the ultimate quality of image registration in radiography," Pattern Recogn. Image Anal. **19**, 63–68 (2009).

[28]M. L. Wilkins, C. F. Cline, and C. A. Honodel, Fourth progress report of light armor program, Technical Report UCRL50694, Lawrence Livermore National Laboratory, University of California, CA, 1969.

[29]D. P. Dandekar, Shock response of boron carbide, Technical Report ARL-TR-2456, Army Research Laboratory, 2001.

[30]G. R. Johnson and T. J. Holmquist, "A computational constitutive model for brittle materials subjected to large strains, high strain rates and high pressures," in *Shock-Wave and High-Strain-Rate Phenomena in Materials* (Marcel Dekker Inc., New York, 1992), pp. 1075–1081.

[31]G. R. Johnson and T. J. Holmquist, "An improved computational constitutive model for brittle materials," AIP Conf. Proc. **309**, 981–984 (1994).

[32]G. R. Johnson, T. J. Holmquist, and S. R. Beissel, "Response of aluminum nitride (including a phase change) to large strains, high strain rates, and high pressures," J. Appl. Phys. **94**, 1639–1646 (2003).

[33]E. L. Lee and C. M. Tarver, "Phenomenological model of shock initiation in heterogeneous explosives," Phys. Fluids **23**, 2362–2372 (1980).

[34]J. K. Dukowicz, "A general, non-iterative Riemann solver for Godunov's method," J. Comput. Phys. **61**, 119–137 (1985).

[35]D. W. Schwendeman, A. K. Kapila, and W. D. Henshaw, "A study of detonation diffraction and failure for a model of compressible two-phase reactive flow," Combust. Theory Modell. **14**, 331–366 (2010).

[36]S. Y. Grigoryev, B. V. Lakatosh, M. S. Krivokorytov, V. V. Zhakhovsky, S. A. Dyachkov, D. K. Ilnitsky, K. P. Migdal, N. A. Inogamov, A. Y. Vinokhodov, V. O. Kompanets, Y. V. Sidelnikov, V. M. Krivtsun, K. N. Koshelev, and V. V. Medvedev, "Expansion and fragmentation of a liquid-metal droplet by a short laser pulse," Phys. Rev. Appl. **10**, 064009 (2018).